Design for additive manufacturing - effects of part orientation, printer selection, and infill density on mechanical properties and production cost

Ruiqi Chen[1], Liseli Baich[2], James Lauer[3], Debbie G. Senesky[1], and Guha Manogharan*[3]

[1]Department of Aeronautics and Astronautics, Stanford University, 496 Lomita Mall, Stanford CA 94305
[2]Department of Mechanical and Industrial Engineering, Youngstown State University, Youngstown OH 44512
[3]Department of Mechanical Engineering, Pennsylvania State University, University Park PA 16803

* Corresponding Author: gum53@psu.edu

Abstract

This original work investigates the influence of infill design, printer selection, and part orientation on the mechanical properties and production cost of parts fabricated using material extrusion additive manufacturing systems. Flexural test specimens are fabricated in both production-grade (Fortus 250mc) and entry-level (MakerBot Replicator 2X) material extrusion systems with varying infill densities (1 mm to 10 mm spacing between rasters). In addition, solid infill specimens are printed in three orientations to establish baseline mechanical stiffness and strength. Finite element simulations and a simplified analytical model based on Euler-Bernoulli beam theory are developed. Results show reasonable agreement between analytical, simulation, and experimental results; 10-20% and 10-40% deviation for production-grade and entry-level specimens specimens, respectively. There is a 40% reduction in stiffness and strength between the solid XY specimen and 1 mm infill specimen. As infill density is further decreased, stiffness and strength asymptotically reduces by 60-70% when compared to solid specimens. This effect is more pronounced in specimens fabricated using entry-level printers, which indicates that printer selection plays a role in printing highly sparse parts. Cost analysis suggests that up to 40% savings can be achieved with highly sparse structures. However, for structural parts, it is recommended that parts be printed with solid infill and with the loading direction aligned in the XY plane to achieve high stiffness, high strength, and reasonable cost. Findings from this study show that there is minimal cost savings but high reduction in mechanical stiffness and strength when sparse infills are used in both production-grade and entry-level printers. Hence, it is recommended that solid infill should be used in all regions of parts that carry significant mechanical stress and sparse infill be used solely to support internal geometries and overhangs.

Keywords: material extrusion, fused filament fabrication, infill density, printer selection, part orientation

1 Introduction

One of the most exciting fields of manufacturing in terms of potential for growth and newfound applications is additive manufacturing (AM). It utilizes layer-by-layer data from a computer-aided design (CAD) model of the part to selectively join materials across multiple layers. This unique approach to manufacturing provides a number of benefits, including processing of a variety of material systems, little-to-no setup, lack of need for fixtures, and economic manufacturing of highly complex, custom, and low volume production parts. These advantages could be attributed to the ever-growing adoption of AM for industrial applications across aerospace, automotive, biomedical, and energy sectors. As listed in ASTM F2792, the seven AM process categories include: material extrusion, vat photo-polymerization, binder jetting, material jetting, sheet lamination, and directed energy deposition. This study focuses on material extrusion AM technology. Material extrusion, shown in Figure 1, is also known as fused deposition modeling (FDM) or fused filament fabrication

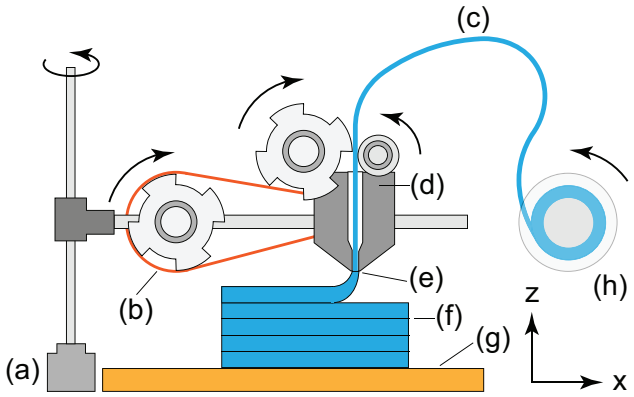

Figure 1: Schematic illustration of a material extrusion 3D printer with (a) z-axis motor and screw drive, (b) x-axis motor and belt drive, (c) feedstock filament, (d) extruder carriage assembly with motor, (e) heated nozzle, (f) printed part, (g) build plate, and (h) filament cartridge.

(FFF). Feedstock (e.g. filament, pellets) is fed into a heated nozle which is controlled using numeric control (NC) to synchronize material extrusion and extruder movement over a build plate. Feedstocks that can be processed through this process range from thermoplastics, wood, metal, carbon-fiber-infused polymers, concrete, food, and biomaterials. Since the expiration of early patents related to material extrusion, the prices for building, operating, and maintaining material extrusion printers has significantly decreased over the past decade [1] and has led to "democratization" of AM [2], with increased adoption in small businesses and schools [3]–[5]. In recent decade, material extrusion has risen to prominence, especially in applications such as education [3], [6], do-it-yourself (DIY) projects, medical implants [7], and rapid prototyping applications that require small-scale custom produced parts [8].

The goal of this work is to evaluate the role of proper infill selection, part orientation, and influence of printer selection on optimal infill density for mechanical part design. Specifically, this study will investigate the effect of printer selection (entry-level versus production-grade), build plane orientation, and infill density on stiffness, strength, and cost of material extrusion AM parts. Four point bending specimens are fabricated using two printers, Fortus (production-grade) and MakerBot (entry-level), and tested to failure to determine effective flexural stiffness and strength. The specimens include solid infills built in three orientations and sparse infills of various densities. Finite element analysis and a simplified analytical model based on Euler-Bernoulli beam theory are developed to correlate the effect of infill density on the effective flexural stiffness. Finally, a cost analysis based on printing time and material consumption is presented to identify implications of infill density selection based on production-grade and entry-level AM systems.

2 Background

Material extrusion AM printers use a heated nozzle to melt and selectively extrude feedstock filament layer-by-layer onto a build plate [2]. The nozzle and build stage are controlled by stepper motors using numerical control. Process planning is conducted by converting a computer aided design (CAD) model of the desired part into NC code for the printer using a "slicer" software. Overhanging surfaces require additional support structures that are removed after build processing. A diagram of a typical material extrusion 3D printer is shown in Figure 1. A major factor in the widespread adoption of material extrusion printers is in the relative ease of installation and operation when compared to other AM technologies. This leads to lower acquisition and operating costs. However, there are still various grades of material extrusion AM systems with variations in machine configuration and processing capabilities. Additional features such as an enclosed heated chamber, high precision stepper motors, in-process monitoring, multiple nozzles, auto-calibration, and dissolvable support structures will increase the cost of material extrusion AM systems but could lead to improvements in overall print quality. Wohlers Associates defines entry-level printers as AM systems with a price of $5,000 or less. A qualitative comparison of entry-level versus production-grade printers is shown in

Table 1: Comparison of typical entry-level and production-grade 3D printers.

	entry-level printer	production-grade printer
Size	Desktop-sized	Refrigerator-sized
Enclosure	Optional	Yes
Heated build plate	Optional	Yes
Filament cartridge	Loose coil	Enclosed canister
Cost	Low ($100-5,000)	High ($5,000-750,000)

Table 1.

Although both AM systems have similar functionality, additional features such as the ones previously mentioned greatly improve dimensional accuracy and reduce part warping due to uneven thermal expansion during the build process [9]. In addition, many feedstock materials are hygroscopic, and moisture in feedstock has been shown to cause bubbles and other print defects [10]. Filaments stored in sealed cartridges in production-grade systems could have better mechanical properties and finish when compared to open spools in entry-level systems.

In addition to printer selection, prior studies have shown that multiple process parameters including: material and support selection [11], nozzle temperature [12], uniformity of extruder and bed temperatures [13], part design [13], layer thickness [14], [15], wall thickness [15], infill pattern [15]–[18], part orientation [19], raster angle [20], and gap between extruded roads [21], will influence the final part stiffness, strength, dimensional accuracy, and production time.

In particular, infill density is a process parameter which can be directly controlled by the user and has a strong influence on part stiffness and strength. Prior studies have shown that parts with sparse infill density are lighter in weight but more compliant and weaker than dense parts [16], [17], [22]. This leads to a tradeoff between material consumption, print duration, and mechanical performance of the part. In summary, it is critical to understand the implications of printer selection, infill density, production consts, and mechanical performance of parts produced through material extrusion AM systems.

3 Methodology

This study focuses on the effect of infill density, part orientation, and printer selection on mechanical behavior and production costs of acrylonitrile butadiene styrene (ABS) polymer material extrusion AM systems. An entry-level printer (MakerBot) and a production-grade printer (Stratasys FDM) are used to fabricate four point bending test specimens with varying infill densities. In addition, solid infill specimens are printed to evaluate the effect of build orientation on mechanical behavior and production cost. Alternating infill pattern of $\pm 45^\circ$ across each layer is evaluated. A simplified analytical model and finite element simulations are used to correlate predicted and experimental results (strength and stiffness) from four point bending experiments. Finally, a cost analysis is presented based on machine usage time and feedstock cost.

3.1 Nominal Specimen Geometry

Per ASTM D6272 [23], nominal four point bending specimens consisting of a 0.762 mm floor (solid bottom layer), 0.762 mm ceiling (solid top layer), 0.5 mm wall thickness (contour), and alternating layers of $\pm 45^\circ$ raster infill of 0.254 mm tall and 0.254 mm thick (total of 20 infill layers per specimen). The spacing between individual infill rasters is varied between 1 mm to 10 mm. The overall nominal specimen dimensions are 120 mm long by 25 mm wide by 6.604 mm thick. All specimens are built with the 120 mm $\times$ 25 mm face along the XY print direction, as shown in Figure 2. In order to ensure that the infill pattern was consistent across both printers, the infill geometry was directly modeled in SolidWorks. A partial exploded view of the specimen is shown in Figure 2 and a cross sectional view is shown in Figure 3. In addition, solid specimens with 100% solid infill, as shown in Figure 4, were printed in all three build orientations (XY, YZ, XZ) on both printers.

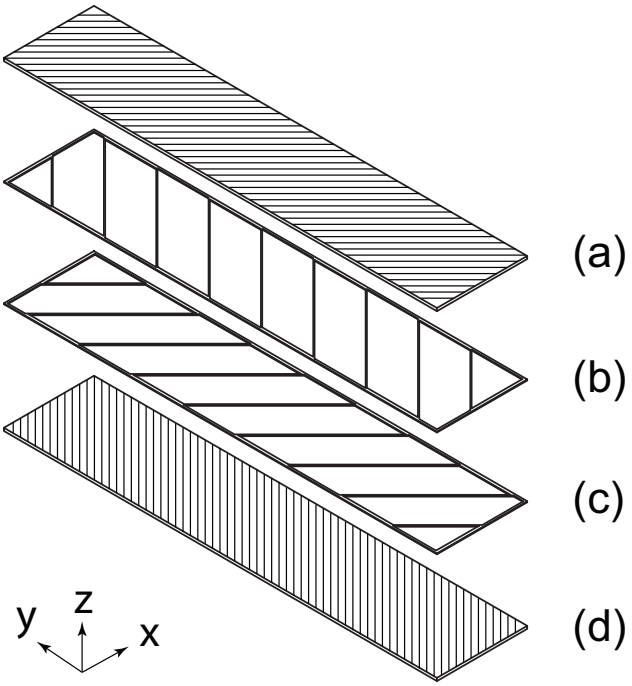

Figure 2: Four point bending specimen: (a) floor, (b) +45° infill, (c) −45° infill, and (d) ceiling layers. There are ten layers of each infill type in alternating sequence for a total of 20 infill layers.

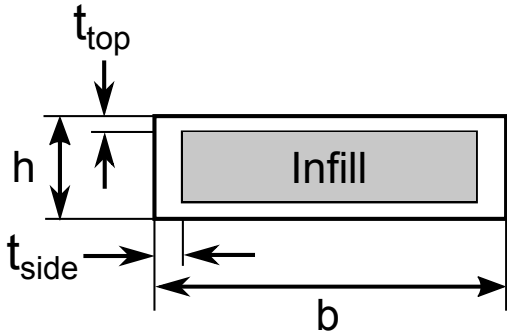

Figure 3: Cross section of bending specimens with infill, where $h = 6.604$ mm, $b = 25$ mm, $t_{top} = 0.762$ mm, and $t_{side} = 0.5$ mm.

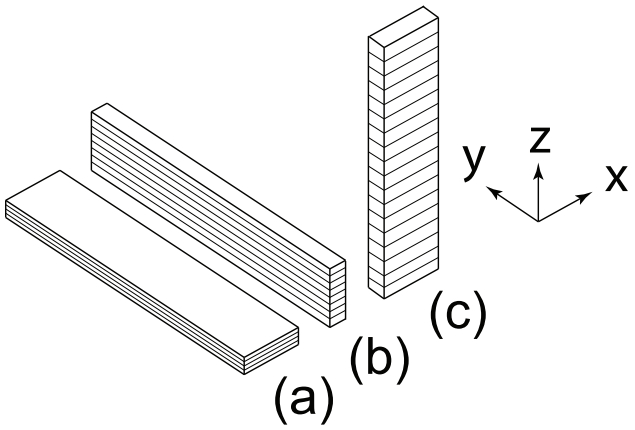

Figure 4: Solid bending specimens in (a) XY, (b) YZ, and (c) XZ planes.

Table 2: Mechanical properties of Fortus and MakerBot feedstock materials.

Property	ABSplus-P430	MakerBot ABS
Ultimate tensile strength (MPa)	33	38
Tensile modulus (MPa)	2200	2320
Elongation at break (%)	6	7
Flexural strength (MPa)	58	59
Compressive strength (MPa)	49	49

3.2 Printer Configuration

The Stratasys Fortus 250mc is a production-grade printer with a 254x254x305 mm build volume. Relevant features of the printer include: heated 254x254 mm build plate, heated enclosure with fan, three layer thickness settings (0.178 mm, 0.254 mm, 0.330 mm), dual nozzle extrusion (ABSplus-P430 filament and SR-30 support material), and proprietary slicing software provided by machine manufacturer (Insight, version 9.0). production-grade specimens are printed using a T14 nozzle tip and a layer thickness of 0.254 mm. File preparation is done using Stratasys's proprietary Insight software. The software automatically selects appropriate temperatures, print speeds, and other process parameters for a given material and with limited user inputs on process conditions and infill patterns.

The MakerBot Replicator 2X is an entry-level printer with a 246x152x155 mm build volume. Relevant features of this printer include: heated 246x152 mm build plate, unheated enclosure with no circulation fan, variable layer thickness (minimum 0.100 mm), dual nozzle extrusion (MakerBot ABS filament), and compatibility with open source slicers (e.g. Cura, Slic3r, MakerBot Desktop). entry-level printer specimens are printed using a 0.4 mm diameter nozzle tip. Build preparation is done using MakerBot's proprietary MakerBot Desktop software (version 3.10). When compared to production-grade systems, entry-level systems (e.g. MakerBot) provides the user with significant control over various process parameters and infill design. In order to normalize production quality across both systems, the layer height is set at 0.25 mm and two contour outer shells are used. By default, the *high quality* setting in MakerBot Desktop places a raft underneath the geometry. The raft provides structural stability and reduces warping caused by the thermal expansion and shrinking of layers as they are deposited and was manually removed from the specimens after they printed.

3.3 Material Properties

The Fortus uses ABSplus-P430 filament feedstock while the MakerBot uses MakerBot ABS filament feedstock, and a summary of corresponding mechanical properties is presented in Table 2.

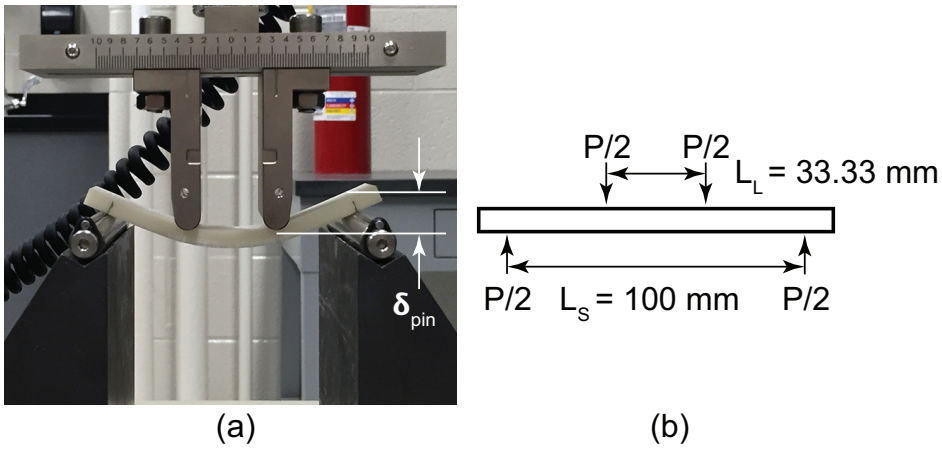

Figure 5: (a) Four point bend test setup. (b) Free body diagram of test setup, where P is the applied load, L_S is the span length, and L_L is the load length.

3.4 Bending Test Setup

The four point bending tests are performed on an Instron Model 5967 universal testing machine using a 30 kN load cell, shown in Figure 5. Per ASTM D6272, a strain rate of 2.96 mm/mm/min is used across all specimens. The support span L_S is set to 100 mm and the load span L_L is set to 33.3 mm. The Instron crosshead displacement is used to measure the displacement of the two upper loading pins.

The effective flexural modulus E_{eff} is defined as the Young's modulus modulus of a solid, homogeneous, isotropic material that would produce the same initial load-displacement response in AM specimens (with the same overall dimensions). Similarly, the effective flexural strength S_{eff} is the maximum bending stress acting on a solid, homogeneous, and isotropic specimen. Based on Euler-Bernoulli beam theory, the load-displacement response for four-point bending is given by

$$\delta_{pin} = \frac{P(L_S - L_L)^2(L_S + 2L_L)}{48 E_{eff} I_{eff}} \tag{1}$$

where δ_{pin} is the displacement measured at the upper loading pin and P is the load applied at both upper loading pins. Since the specimens have a rectangular cross section with width b and thickness d, the effective second moment of area I_{eff} is given by

$$I_{eff} = \frac{bd^3}{12} \tag{2}$$

Substituting Equation 2 and the relation $L_S = 3L_L$ into Equation 1 provides

$$\begin{aligned} E_{eff} &= \frac{5}{27}\frac{P}{\delta_{pin}}\frac{L_S^3}{bd^3} \\ &\approx 0.185\frac{mL_S^3}{bd^3} \end{aligned} \tag{3}$$

where m is the slope of the measured load-displacement response in the linear region. It should be noted that this is an estimate based on displacement measurements at the upper loading pin and not at the center of the beam. The effective flexural strength is given by

$$S_{eff} = \frac{P_{max} L_S}{bd^2} \tag{4}$$

where P_{max} is the maximum load recorded during experimentation.

3.5 Finite Element Analysis

Finite element analysis (FEA) is a commonly employed method to predict the flexural stiffness of specimens, including AM specimens [24]–[26]. The nominal geometry described in Section 3.1 is simulated in Abaqus (version 6.12) using S4R shell elements for the infill specimens. In addition, an outer shell model consisting of floor, ceiling, and contour walls (i.e. no infill) is also modeled for reference. In the case of solid specimens, a 3D model consisting of C3D8R brick elements is used, without distinction across multiple build orientations in the simulation. A linearelastic material is used based on Young's modulus presented in Section 3.3. Since Poisson ratio is not provided in the material datasheets, a value of $\nu = 0.35$ is assumed [27]. Displacement boundary conditions in the vertical direction are applied at the line of nodes to represent the top roller pins in a four-point bend setup. Pinned and roller boundary conditions are applied at the line of nodes for the bottom roller pins. The effective flexural modulus is calculated using Equation 7, where P and δ are results from the simulation. Effective flexural strength was not simulated due to the lack of material properties in the plastic regime.

3.6 Simplified Analytical Solution

In addition to experimentation and FEA, a simple analytical model based on Euler-Bernoulli beam theory is developed. In the case of solid specimens, the effective flexural modulus and strength are expected to match the bulk material results. In the case of infill specimens, the infills are neglected in the simplified model and only the top, bottom, and side shells are considered. The maximum deflection δ_{center} of a beam under four-point-bending is given by

$$\delta_{center} = \frac{P(2L_S^3 - 3L_L^2 L_S + L_L^3)}{96EI} \tag{5}$$

where P is the applied load from two points (with each point contributing $P/2$), E is the Young's modulus of the bulk material, I is the second moment of area, L_L is the load span, and L_S is the support span, as shown in Figure 5. In order to find the effective flexural modulus E_{eff}, the cross section is assumed to be solid, and therefore the effective second moment of area is given by

$$I_{eff} = \frac{bh^3}{12} \tag{6}$$

where b is the beam width and h is the beam height (thickness). Substituting E_{eff} and I_{eff} into Equation 5 and rearranging yields

$$E_{eff} = \frac{P(2L_S^3 - 3L_L^2 L_S + L_L^3)}{8\delta bh^3} \tag{7}$$

Finally, substituting the ratio P/δ from Equation 5 (which considers the true Young's modulus E and second moment of area I) into Equation 7 provides

$$\begin{aligned} E_{eff} &= \frac{12EI}{bh^3} \\ &= E\frac{I}{I_{eff}} \end{aligned} \tag{8}$$

Based on the cross section of the beam shown in Figure 3, the second moment of area (I) can be written as

$$I = \frac{bh^3}{12} - \frac{(b - 2t_{side})(h - 2t_{top})^3}{12} \tag{9}$$

Using nominal cross section dimensions from Section 3.1 and material properties from Section 3.3, the second moment of area is 326 mm^4 and the effective flexural stiffness is $0.570 \times E$, or 1254 MPa for the Fortus ABSplus-P430 material and 1322 MPa for the MakerBot ABS material.

Table 3: Simulated effective flexural modulus values.

Infill	E_{eff}, production-grade (MPa)	E_{eff}, entry-level (MPa)
Solid	2170	2288
1 mm	1063	1121
3 mm	1014	1069
4 mm	1009	1064
6 mm	1004	1059
10 mm	1003	1057
None	999	1053

3.7 Print Time and Production Cost Analysis

A print time and production cost analysis is performed by using the print time and feedstock volume required, as estimated by Insight and MakerBot Desktop for Fortus and MakerBot, respectively. The unit cost of ABSplus-P430 is estimated at \$0.00028/mm^3 based on \$260 per spool with a volume of 922600 mm^3, while the unit cost of MakerBot ABS is estimated at \$0.000045/mm^3 based \$43 per spool with a volume of 961538 mm^3. Machine usage cost rates for Fortus and MakerBot are estimated to be \$0.50/min and \$0.17/min, respectively. These rates are based on a prior analysis conducted by Baich et al. [16]. A simplified model for the total part cost is therefore given by

$$C_{total} = T \times C_{usage} + V \times C_{feedstock} \tag{10}$$

where C_{total} is the total part cost (\$), T is the print time (min), C_{usage} is the machine usage cost per minute, V is the feedstock volume (mm^3), and $C_{feedstock}$ is the feedstock cost per mm^3.

4 Results and Discussion

4.1 Finite Element Analysis

Results for the simulated effective flexural modulus across all infill densities and build directions are presented in Table 3. A mesh size of 0.12 mm was used for all shell element simulations. Mesh convergence was tested using a smaller mesh size of 0.08 mm, which yielded less than 0.3% difference in simulated flexural stiffness. In the case of solid brick elements, a mesh size of 1 mm was used. Mesh convergence was tested using a smaller mesh size of 0.5 mm, yielding less than 1.4% difference in simulated flexural stiffness. The simulated modulus values are lower than the analytical results due to additional deformation modes in shell elements that are not present in the simplified Euler-Bernoulli beam model. The simulations also suggest that the infill has negligible effect on the effective flexural modulus. This can be attributed to the distribution of bending stress across both floor and ceiling layers with the infill acting as a separator between these two surfaces, akin to a sandwich panel structure.

4.2 Four-Point Bending Experiments

Three of each specimen type was printed using both the entry-level and production-grade printers. Several representative specimens (partially printed) are shown in Figure 6. Overall specimen length, width, and thickness were measured ($n = 3$) with digital calipers before testing. A summary of experimental results for four point bending is given in Table 4. Experimental and simulated effective flexural modulus are presented in Figure 7. Experimental flexural strength is presented in Figure 8. Simulated and experimental flexural modulus are in reasonable agreement (10-20% error). This error is more pronounced in entry-level specimens as detailed in Section 4.2.2.

4.2.1 Effect of Build Orientation on Mechanical Behavior

As observed in Figure 7, FEA simulations overestimate the effective flexural modulus for the solid specimens. Since anisotropic behavior due to build direction is not accounted for in the FEA, the deviation is

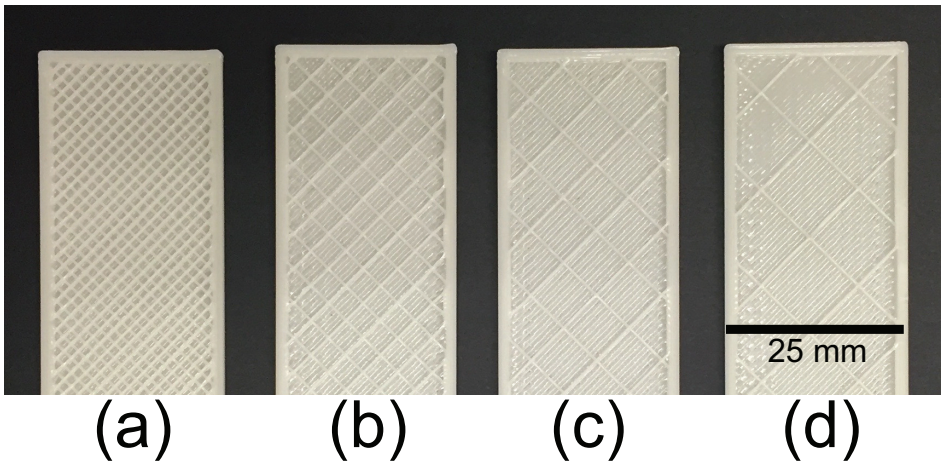

Figure 6: Representative four point bending specimens with (a) 1 mm, (b) 3 mm, (c) 6 mm, and (d) 10 mm infill. Top layer (ceiling) was not printed to show infill.

Table 4: Effective flexural strength and effective modulus of elasticity for production-grade and entry-level specimens. S.D. indicates standard deviation.

	production-grade		entry-level	
Infill	Strength ± S.D. (MPa)	Modulus ± S.D. (MPa)	Strength ± S.D. (MPa)	Modulus ± S.D. (MPa)
Solid XY	44.2 ± 0.4	1931 ± 52	47.5 ± 1.0	1814 ± 38
Solid YZ	52.7 ± 2.0	1913 ± 32	49.1 ± 0.7	2034 ± 30
Solid XZ	36.5 ± 0.4	1731 ± 30	26.4 ± 3.4	1734 ± 143
1 mm	25.1 ± 0.8	1085 ± 44	22.7 ± 1.4	1057 ± 29
3 mm	22.8 ± 0.7	1025 ± 18	17.8 ± 2.8	855 ± 25
4 mm	19.9 ± 0.6	916 ± 7	16.9 ± 0.5	834 ± 23
6 mm	18.5 ± 0.8	869 ± 25	13.7 ± 0.7	770 ± 18
10 mm	16.0 ± 0.1	928 ± 45	15.1 ± 0.2	771 ± 32

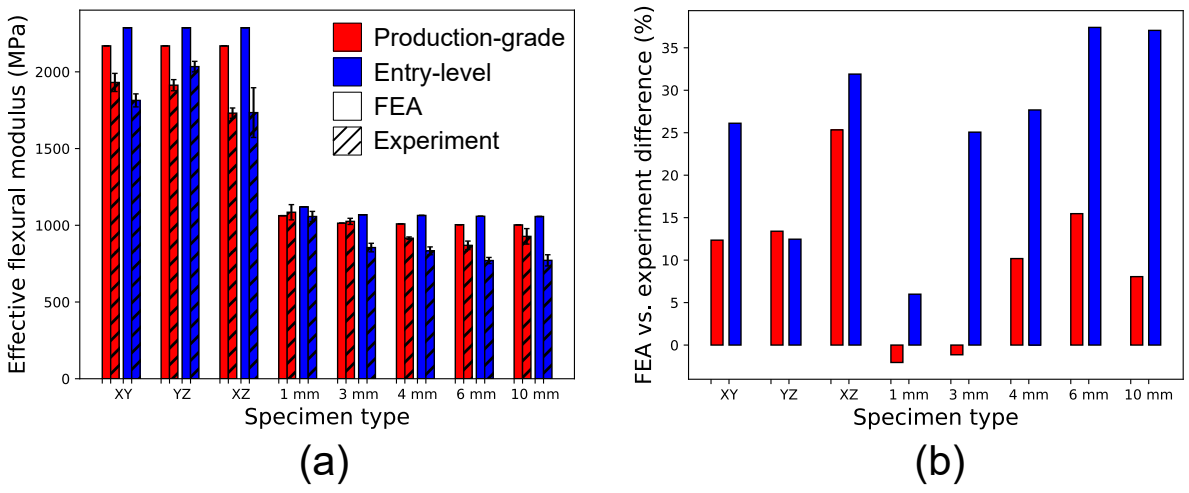

Figure 7: (a) Simulation and experimental results of flexural modulus. (b) Percent difference between simulated and experimental flexural modulus.

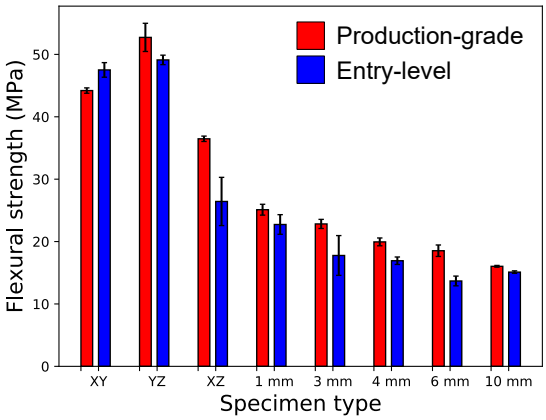

Figure 8: Experimental results of flexural strength.

much larger for the XZ oriented specimen. This anisotropic behavior may be due to voids between adjacent roads that decrease the effective modulus of the as-printed material [28]–[30]. It may also be caused by changes in melting and re-solidification of the filament material itself as it is exposed to the high temperature nozzle [31], [32]. In addition, the XY and YZ specimens have continuously deposited raster infills along the beam axis when compared to XZ specimens with infills that are perpendicular to the beam axis. These continuously deposited parallel raster infills carry bending loads more effectively compared to the perpendicular infills [15], [33].

Similar trends are observed in the effective flexural strength, where the XZ specimens have the lowest flexural strength due to presence of voids and gaps between extruded rasters, which lead to stress concentrations [15]. In addition, prior work has shown that factors such as extruder temperature [12], build chamber temperature [34], [35], and print speed [36] affect the formation of bonds and degree of wetting between adjacent rasters.

4.2.2 Effect of Infill Density on Mechanical Behavior

Simulation results correlate with experimental results where the effective flexural modulus decreases with reduction in infill density. However, this trend is more significant in the entry-level system compared to the production-grade system. At very low infill densities, the FEA simulations predict that the infill has negligible impact on the effective flexural stiffness. This result is observed in the production-grade specimens, with the 4 mm through 10 mm specimens having nearly the same effective flexural stiffness. However, for the entry-level specimens, the effective flexural stiffness continues to decrease as infill density decreases. The different trends across these two printers could be attributed to geometric distortion and sagging of the ceiling in entry-level systems. The production-grade system has a heated build enclosure with circulation fan to improve convective heat transfer in the build environment, which reduces thermal warping. In addition, when the infill density is low, the solid rasters in the ceiling are largely unsupported. It is hypothesized that production-grade systems use more optimal process parameters (e.g. speed, nozzle temperature, filament retraction) to reduce warping and geometric distortion in unsupported structures compared to entry-level systems. Finally, overall differences in printer hardware and printer build quality may also contribute to major variations in dimensional accuracy and reliability [5], [37], which would contribute to lower flexural modulus in entry-level specimens.

The infill density also has a dramatic impact on flexural strength in both production-grade and entry-level specimens, with lower infill densities resulting in lower flexural strength. These results are expected and agree with other similar studies [38]–[40]. Since the infill primarily serves as a separator between the ceiling and floor layers, a lower density provides lesser support for these two load bearing layers. entry-level infill specimens exhibit much lower flexural strength when compared to production-grade specimens (except for solid XY specimen), although both material feedstocks have very similar flexural and compressive

Table 5: Print time and feedstock volume estimates for production-grade and entry-level specimens.

	production-grade			entry-level		
Infill	Print time (min)	Volume (mm^3)	Cost ($)	Print time (min)	Volume (mm^3)	Cost ($)
Solid XY	46	19600	28.52	76	28130	13.92
Solid YZ	83	19480	46.99	76	25810	13.82
Solid XZ	94	19230	52.42	74	24460	13.43
1 mm	36	10940	21.08	68	16820	12.09
3 mm	30	8800	17.48	51	13230	9.09
4 mm	29	8560	16.91	47	12540	8.39
6 mm	28	8080	16.28	45	12210	8.05
10 mm	27	7750	15.68	41	11460	7.35

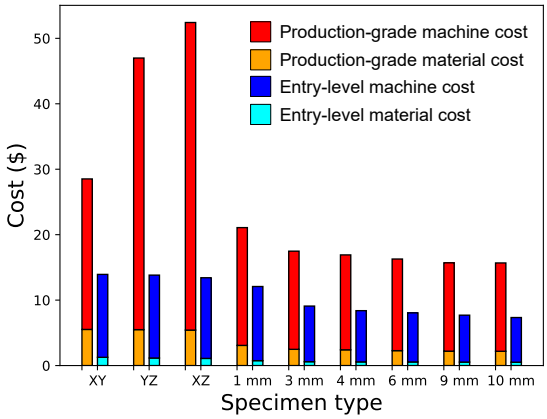

Figure 9: Machine usage cost and material cost for flexural specimens.

strengths (see Table 2). This is likely due to defects in the specimens caused by aforementioned differences in build environment, slicer optimization, printer hardware, and printer build quality. This difference is very pronounced in the solid XZ specimen, where production-grade specimens are 38% stronger than entry-level specimens.

4.3 Time and Cost Analysis

A summary of print time, feedstock volume, and total cost is detailed in Table 5. Cost components in both entry-level and production-grade systems are presented in Figure 9. Lower infill density results in decreases in print time, volume, and production cost. entry-level specimens have longer print time and use more feedstock material due to the presense of a raft. The orientation of the specimens also has a major effect on print time and production cost in production-grade specimens, with XZ specimens taking 104% longer to print and being 84% more expensive than XY specimens. In the case of entry-level system, there is no noticeable differences in time and cost for the solid specimens. This indicates that the slicing software for the production-grade system is likely optimizing print speed, filament retraction, and possibly other settings based on build orientation, which can lead to dramatic differences in print time.

4.3.1 Mechanical Performance versus Cost

As shown in Figure 10, analysis of flexural stiffness and strength as a function of total production cost identifies clear clusters of specimens that are printer-dependent. All three entry-level solid specimens have very similar costs, but there is a wide variation in mechanical performance between the XZ and YZ

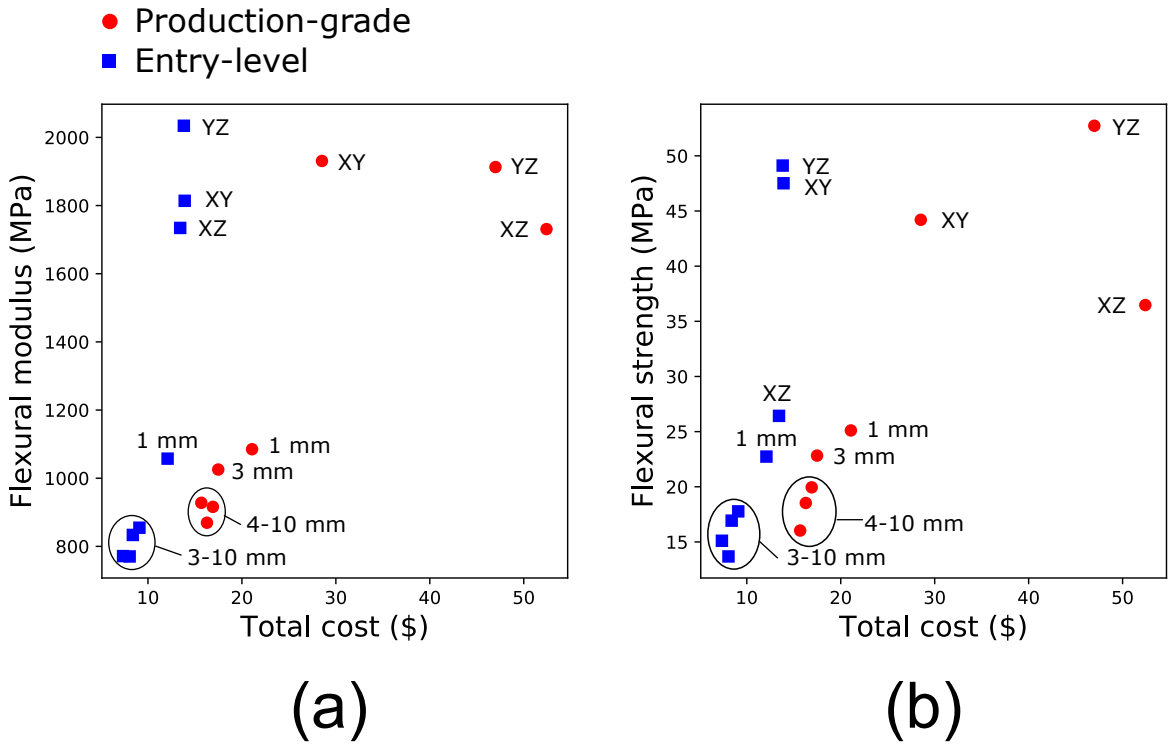

Figure 10: Total production cost as a function of (a) flexural modulus and (b) flexural strength for entry-level and production-grade specimens.

specimens, which is reflective of aligning solid continuous rasters along the applied loading direction. In the case of production-grade system, the solid specimens have a wide variation in production costs, which is reflective of higher operating costs and print times. In particular, the XZ and YZ specimens are 84% and 65% more expensive than the XY specimen, respectively. However, the YZ and XY specimens have very similar mechanical properties, indicating that printing in the XY plane is preferable for optimal mechanical properties at lower cost.

In addition, it can be observed from Figure 10 that the infill specimens cluster around lower production cost at decreased mechanical performance. It should be noted that the solid XY specimens are 35% and 15% more expensive than the 1 mm infill specimens for production-grade and entry-level systems, respectively. However, the solid XY specimens are 78% and 67% stiffer than the 1 mm infill specimens for production-grade and entry-level systems, respectively. Similarly, the solid XY specimens are 76% and 109% stronger than the 1 mm infill specimens for production-grade and entry-level systems, respectively. This major finding indicates that modest increases in production cost can result in substantial increases in mechanical performance, i.e. solid parts could be more optimal than parts with even 1 mm infill density. Sparser infill specimens such as the 4 mm through 10 mm specimens generally cluster together in Figure 10, which indicates that there is minimal difference in cost or mechanical performance between these specimens, especially when compared to the solid specimens.

Cost savings, reduction in stiffness, and reduction in strength relative to the solid XY specimen are shown in Figure 11. The XY solid specimen is chosen as the reference specimen since all the infill specimens are manufactured in the XY plane. As shown in Figure 11, the lowest infill density can lead to roughly 45% cost savings. However, stiffness is reduced by around 55%, and strength is reduced by around 65%. If cost is the *only* concern, then printing parts with very low infill densities can lead to significant cost savings. However, if mechanical considerations are important, then printing solid parts oriented with loading in the XY plane leads to excellent stiffness and strength at modest costs.

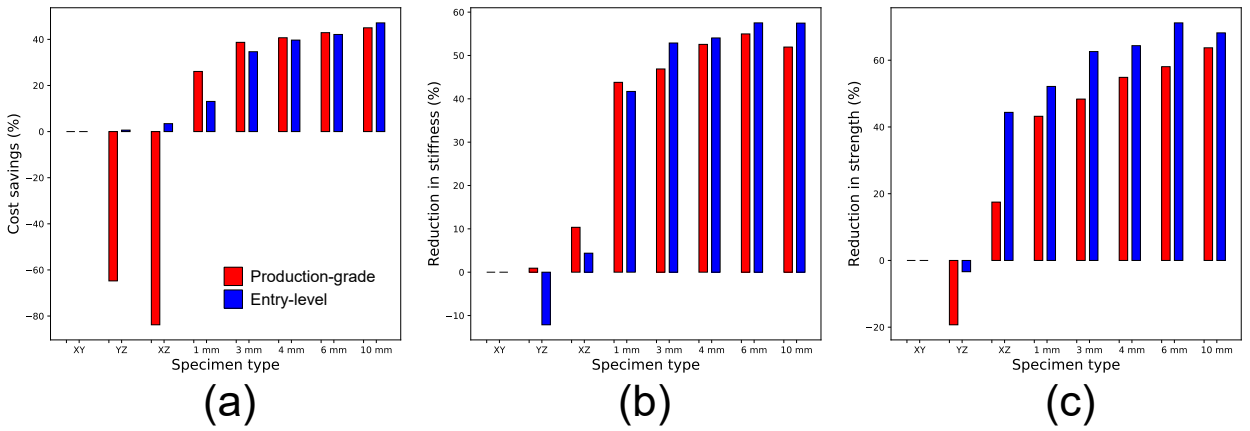

Figure 11: Effect of infill type on (a) cost, (b) stiffness, and (c) strength reduction. All values are calculated with reference to the XY solid specimen.

4.4 Implications

This study has shown that part orientation, printer selection, and infill density, part orientation, and printer selection all have an impact on the mechanical behavior and production cost of flexural test specimens. These results can be generalized and applied to other parts and geometries printed using material extrusion AM systems.

Part orientation has a significant impact on mechanical stiffness and strength of parts manufactured using material extrusion AM. Extruded rasters are much more efficient at carrying loads when applied loads and stresses run parallel to the raster extrusion paths. In addition, continuous rasters lead to higher stiffness and strength compared to discontinuous rasters. Therefore, it is extremely important to be cognisant of loading direction with respect to the build direction. Ideally, parts should be aligned such that significant load paths lie in the XY plane of the printer. Parts should not be oriented with loading or large features along the build direction, as this leads to deficient mechanical properties and high costs. Proper part orientation is especially important when manufacturing parts on entry-level systems because they lack features such as heated enclosures, leading to worse mechanical properties along the build direction compared to production-grade systems.

Printer selection also has an impact on mechanical behavior and manufacturing cost. In general, parts manufactured on production-grade systems have better mechanical properties compared to parts manufactured on entry-level systems due to better build environment conditions, printer hardware quality, and slicer optimization. However, production-grade parts are also more expensive, with higher machine usage costs being the most significant driver. In addition, production-grade systems have limited options when it comes to infill geometry, layer height, and other custom options. In comparison, entry-level systems typically give users flexibility in choosing and fine tuning process parameters. Many slicing software, such as Cura and Slic3r, are open source, allowing the additive manufacturing community to modify and introduce new features, infill geometries, and slicing algorithms. Several entry-level systems, including RepRap and LulzBot, are also open source, allowing users to add and modify hardware to improve printer quality, support new material systems, and extend printer capabilities beyond the base model. Lower acquisition cost for entry-level systems also makes them much more accessible to schools, small businesses, and hobbyists.

Finally, infill density has a strong impact on mechanical properties, with higher infill density parts having higher mechanical stiffness and strength. However, there is a significant difference in mechanical properties between solid infill and 1 mm infill. For parts under mechanical loading, solid infills should be used for all regions of the part that carry mechanical stresses. Sparse infills should only be used in non-structural regions and only for supporting internal geometries and overhangs as they provide negligible mechanical benefits.

While this work only investigates $\pm 45°$ alternating raster infills, other infill patterns such as ones based on Hilbert curves [41] should be investigated to see if cost reductions can be achieved by reducing extruder

travel distance. In addition, other solid infill types such as stress tensor aligned infill [42] should also be investigated to see if better mechanical properties can be achieved.

5 Conclusion

This work addresses how part orientation, printer selection, and infill density affect the mechanical properties and production cost of parts manufactured using material extrusion AM systems. Four point bending specimens with solid and sparse infill are fabricated using both a production-grade printer and an entry-level printer. The solid infill specimens are fabricated in multiple build orientations and the sparse infill specimens are manufactured using several infill densities. A simplified analytical model based on Euler-Bernoulli beam theory and finite element simulations are used to corroborate the experimental results. In addition, a cost analysis based on material feedstock cost and machine usage cost is developed. The results of this work show that:

- Build orientation has a strong influence on part stiffness and strength for both entry-level and production-grade AM systems. For production-grade systems, build orientation can dramatically increase the machine usage cost. For best mechanical performance, parts manufactured using material extrusion AM systems should be oriented such that load and stress paths are preferentially aligned in the XY plane of the printer.
- Parts produced using production-grade AM systems generally have superior mechanical properties compared to ones produced using entry-level systems. However, they are more expensive due to high machine usage costs and less flexible in terms of process parameters. entry-level systems, on the other hand, are significantly cheaper to acquire and frequently support open source hardware and slicing software to allow precise control of process parameters, which allows the AM community to actively and openly develop new features and tools.
- Infill density has a significant impact on mechanical properties. Switching from a solid infill to a 1 mm sparse infill leads to dramatic reductions in mechanical stiffness and strength without much cost savings. Hence, it is recommended that solid infills be used in all regions of parts that carry significant mechanical stress, while sparse infills be used solely to support internal geometries and overhangs.

Several aspects that require further investigation include alternative infill generation techniques that may lead to superior mechanical properties or lower production costs. In addition, a wider survey of entry-level and production-grade AM systems is necessary to expand beyond the two specific printers considered in this study. A review by Popescu showed that the generalization of process parameters and results from printer to printer is limited due to wide differences in how printers implement process parameters and slicing algorithms [40]. Further research is necessary to determine how various process parameters affect the dimensional accuracy of highly sparse infill parts and unsupported structures. While the present work has shown that differences exist in this area with respect to production-grade and entry-level printers, specific factors have not been conclusively identified, primarily due to the lack of openness in the production-grade software. A deeper understanding in this area may help identify what process parameters contribute most to successful part construction and print reliability. Finally, the ideal infill type, density, and printer orientation for a given part is highly loading dependent. While this work and complementary work by Baich [16] focus on tensile, compressive, and bending loads, more studies are needed on other loading conditions such as shear, torsion, and equibiaxial loading.

Conflicts of Interest

The authors declare no conflicts of interest.

Acknowledgments

The authors would like to acknowledge the Structures and Composites Laboratory (SACL) at Stanford University for providing assistance in performing finite element analysis. Ruiqi Chen would like to thank the

National Defense Science and Engineering Fellowship (NDSEG) program as well as the Stanford Graduate Fellowship (SGF) program for their generous and continuous support over the years.

References

[1] C. Weller, R. Kleer, and F. T. Piller, "Economic implications of 3d printing: Market structure models in light of additive manufacturing revisited," *International Journal of Production Economics*, vol. 164, pp. 43–56, 2015.

[2] R. Jones, P. Haufe, E. Sells, P. Iravani, V. Olliver, C. Palmer, and A. Bowyer, "Reprap–the replicating rapid prototyper," *Robotica*, vol. 29, no. 1, pp. 177–191, 2011.

[3] C. Schelly, G. Anzalone, B. Wijnen, and J. M. Pearce, "Open-source 3-d printing technologies for education: Bringing additive manufacturing to the classroom," *Journal of Visual Languages & Computing*, vol. 28, pp. 226–237, 2015.

[4] A. Laplume, G. C. Anzalone, and J. M. Pearce, "Open-source, self-replicating 3-d printer factory for small-business manufacturing," *The International Journal of Advanced Manufacturing Technology*, vol. 85, no. 1-4, pp. 633–642, 2016.

[5] B. P. Conner, G. P. Manogharan, and K. L. Meyers, "An assessment of implementation of entry-level 3d printers from the perspective of small businesses," *Rapid Prototyping Journal*, 2015.

[6] Y. AbouHashem, M. Dayal, S. Savanah, and G. Strkalj, "The application of 3d printing in anatomy education," *Medical education online*, vol. 20, no. 1, p. 29 847, 2015.

[7] D. Espalin, K. Arcaute, D. Rodriguez, F. Medina, M. Posner, and R. Wicker, "Fused deposition modeling of patient-specific polymethylmethacrylate implants," *Rapid Prototyping Journal*, vol. 16, no. 3, pp. 164–173, 2010.

[8] I. Campbell, D. Bourell, and I. Gibson, "Additive manufacturing: Rapid prototyping comes of age," *Rapid prototyping journal*, 2012.

[9] K. Singh, "Experimental study to prevent the warping of 3d models in fused deposition modeling," *International Journal of Plastics Technology*, vol. 22, no. 1, pp. 177–184, 2018.

[10] E. Kim, Y.-J. Shin, and S.-H. Ahn, "The effects of moisture and temperature on the mechanical properties of additive manufacturing components: Fused deposition modeling," *Rapid Prototyping Journal*, vol. 22, no. 6, pp. 887–894, 2016.

[11] F. Fischer, "Thermoplastics: The best choice for 3d printing," *White Paper, Stratasys Inc., Edn Prairie, MN*, 2011.

[12] N. Aliheidari, J. Christ, R. Tripuraneni, S. Nadimpalli, and A. Ameli, "Interlayer adhesion and fracture resistance of polymers printed through melt extrusion additive manufacturing process," *Materials & Design*, vol. 156, pp. 351–361, 2018.

[13] P. K. Gurrala and S. P. Regalla, "Part strength evolution with bonding between filaments in fused deposition modelling: This paper studies how coalescence of filaments contributes to the strength of final fdm part," *Virtual and Physical Prototyping*, vol. 9, no. 3, pp. 141–149, 2014.

[14] A. Boschetto and L. Bottini, "Accuracy prediction in fused deposition modeling," *The international journal of advanced manufacturing technology*, vol. 73, no. 5-8, pp. 913–928, 2014.

[15] A. K. Sood, R. K. Ohdar, and S. S. Mahapatra, "Parametric appraisal of mechanical property of fused deposition modelling processed parts," *Materials & Design*, vol. 31, no. 1, pp. 287–295, 2010.

[16] L. Baich, G. Manogharan, and H. Marie, "Study of infill print design on production cost-time of 3d printed abs parts," *International Journal of Rapid Manufacturing*, vol. 5, no. 3-4, pp. 308–319, 2015.

[17] M. Fernandez-Vicente, W. Calle, S. Ferrandiz, and A. Conejero, "Effect of infill parameters on tensile mechanical behavior in desktop 3d printing," *3D printing and additive manufacturing*, vol. 3, no. 3, pp. 183–192, 2016.

[18] O. Iyibilgin, M. Leu, G. Taylor, H. Li, and K. Chandrashekhara, "Investigation of sparse-build rapid tooling by fused deposition modeling," in *Proceedings of the 25th International Solid Freedom Fabrication Symposium on Additive Manufacturing*, 2014, pp. 4–6.

[19] A. M. Phatak and S. Pande, "Optimum part orientation in rapid prototyping using genetic algorithm," *Journal of manufacturing systems*, vol. 31, no. 4, pp. 395–402, 2012.

[20] C. McIlroy and P. Olmsted, "Disentanglement effects on welding behaviour of polymer melts during the fused-filament-fabrication method for additive manufacturing," *Polymer*, vol. 123, pp. 376–391, 2017.

[21] D. Ahn, J.-H. Kweon, S. Kwon, J. Song, and S. Lee, "Representation of surface roughness in fused deposition modeling," *Journal of Materials Processing Technology*, vol. 209, no. 15-16, pp. 5593–5600, 2009.

[22] C. Alvarez, L. Kenny, C. Lagos, F. Rodrigo, and M. Aizpun, "Investigating the influence of infill percentage on the mechanical properties of fused deposition modelled abs parts," *Ingenieria e Investigacion*, vol. 36, no. 3, pp. 110–116, 2016.

[23] ASTM International, *Standard test method for flexural properties of unreinforced and reinforced plastics and electrical insulating materials by four-point bending*, 2017.

[24] M. Domingo-Espin, J. M. Puigoriol-Forcada, A.-A. Garcia-Granada, J. Llumà, S. Borros, and G. Reyes, "Mechanical property characterization and simulation of fused deposition modeling polycarbonate parts," *Materials & Design*, vol. 83, pp. 670–677, 2015.

[25] G. Taylor, X. Wang, L. Mason, M. C. Leu, K. Chandrashekhara, T. Schniepp, and R. Jones, "Flexural behavior of additively manufactured ultem 1010: Experiment and simulation," *Rapid Prototyping Journal*, 2018.

[26] M. Somireddy, D. A. De Moraes, and A. Czekanski, "Flexural behavior of fdm parts: Experimental, analytical and numerical study," in *Proceedings of the 28th Annual International Solid Freeform Fabrication Symposium—An Additive Manufacturing Conference, Austin, TX, USA*, 2012, pp. 7–9.

[27] *Mechanical properties of plastic materials*, `https://web.archive.org/web/20170802144914/http://www.professionalplastics.com/professionalplastics/MechanicalPropertiesofPlastics.pdf`, Accessed: 2020-01-06.

[28] L. Li, Q. Sun, C. Bellehumeur, and P. Gu, "Composite modeling and analysis for fabrication of fdm prototypes with locally controlled properties," *Journal of manufacturing processes*, vol. 4, no. 2, pp. 129–141, 2002.

[29] J. F. Rodriguez, J. P. Thomas, and J. E. Renaud, "Mechanical behavior of acrylonitrile butadiene styrene fused deposition materials modeling," *Rapid Prototyping Journal*, 2003.

[30] R. Chen and D. Senesky, "Effective in-plane moduli of fused filament fabrication material with aligned mesostructure," *JOM*, pp. 1–10, 2019.

[31] J. F. Rodriguez, J. P. Thomas, and J. E. Renaud, "Mechanical behavior of acrylonitrile butadiene styrene (abs) fused deposition materials. experimental investigation," *Rapid Prototyping Journal*, 2001.

[32] A. Bellini and S. Guceri, "Mechanical characterization of parts fabricated using fused deposition modeling," *Rapid Prototyping Journal*, 2003.

[33] B. Akhoundi and A. Behravesh, "Effect of filling pattern on the tensile and flexural mechanical properties of fdm 3d printed products," *Experimental Mechanics*, vol. 59, no. 6, pp. 883–897, 2019.

[34] C. Bellehumeur, L. Li, Q. Sun, and P. Gu, "Modeling of bond formation between polymer filaments in the fused deposition modeling process," *Journal of Manufacturing Processes*, vol. 6, no. 2, pp. 170–178, 2004.

[35] Q. Sun, G. Rizvi, C. Bellehumeur, and P. Gu, "Effect of processing conditions on the bonding quality of fdm polymer filaments," *Rapid Prototyping Journal*, 2008.

[36] K. J. Christiyan, U. Chandrasekhar, and K. Venkateswarlu, "A study on the influence of process parameters on the mechanical properties of 3d printed abs composite," in *IOP Conference Series: Materials Science and Engineering*, IOP Publishing, vol. 114, 2016, p. 012 109.

[37] G. W. Melenka, J. S. Schofield, M. R. Dawson, and J. P. Carey, "Evaluation of dimensional accuracy and material properties of the makerbot 3d desktop printer," *Rapid Prototyping Journal*, 2015.

[38] J. Porter, T. Cain, S. Fox, and P. Harvey, "Influence of infill properties on flexural rigidity of 3d-printed structural members," *Virtual and physical prototyping*, vol. 14, no. 2, pp. 148–159, 2019.

[39] O. Luzanin, V. Guduric, I. Ristic, and S. Muhic, "Investigating impact of five build parameters on the maximum flexural force in fdm specimens–a definitive screening design approach," *Rapid Prototyping Journal*, 2017.

[40] D. Popescu, A. Zapciu, C. Amza, F. Baciu, and R. Marinescu, "Fdm process parameters influence over the mechanical properties of polymer specimens: A review," *Polymer Testing*, vol. 69, pp. 157–166, 2018.

[41] A. Papacharalampopoulos, H. Bikas, and P. Stavropoulos, "Path planning for the infill of 3d printed parts utilizing hilbert curves," *Procedia Manufacturing*, vol. 21, pp. 757–764, 2018.

[42] J. A. Gopsill, J. Shindler, and B. J. Hicks, "Using finite element analysis to influence the infill design of fused deposition modelled parts," *Progress in Additive Manufacturing*, vol. 3, no. 3, pp. 145–163, 2018.